Chapter 5

86 GHz SiO maser survey of late-type stars in the Inner Galaxy IV. Bolometric magnitudes

M. Messineo, H. J. Habing, K. M. Menten, A. Omont, L. O. Sjouwerman

Abstract

We present a study of DENIS, 2MASS, ISOGAL and MSX photometry for a sample of evolved late–type stars in the inner Galaxy, which we previously searched for 86 GHz SiO maser emission (Messineo et al. 2002). Bolometric magnitudes are computed for each SiO star by direct integration of the observed energy distribution, and bolometric corrections as a function of colours are derived. Adopting a distance of 8 kpc the SiO stars within 5° from the Galactic Centre show a distribution of bolometric magnitudes that peaks at $M_{\rm bol} = -5.1$ mag, i.e., very similar to the OH/IR stars close to the Galactic centre. From their bolometric luminosities and interstellar extinction we find that 11% of the SiO stars are likely to be foreground to the bulge. Furthermore the small velocity dispersions of those foreground stars suggest a disk component. The 15 known large amplitude variables included in our sample fall above the Mira period–luminosity relation of Glass et al. (1995), which suggests a steepening of the period–luminosity relation for periods larger than 450 days, as also seen in the Magellanic Clouds. From this period–luminosity relation and from their colours, the envelopes of SiO stars appear less evolved than those of OH/IR stars, which have thicker shells due to higher mass–loss rates.

5.1 Introduction

The early 1960's observations of non-circular gas motions in the inner Galaxy produced evidence for the existence of a Galactic bar (de Vaucouleurs 1964). Its existence is also supported by an apparent asymmetry of the integrated light as seen in COBE maps (Blitz & Spergel 1991) and of the stellar counts (Nakada et al.

Astronomy and Astrophysics (2004), in preparation

1991). Thus, stellar kinematic studies provided less stringent constraints, due to the small number of measured stellar radial velocities. OH and SiO maser emission lines from the envelopes of evolved late-type stars can measure stellar line-of-sight velocities with an accuracy of a few $\mathrm{km\,s^{-1}}$ throughout the Galaxy. Maser emission thereby provides a ready means to measure line-of-sight velocities in the Galactic plane even where the optical interstellar extinction is high.

Lewis (1989) analysed the colours and maser emission of IRAS sources, suggesting a chronological sequence of increasing mass-loss from SiO, to H_2O and OH maser emission. This sequence links AGB stars through the Mira and OH/IR stages with Planetary Nebulae. The presence of particular maser lines apparently depends on the envelope's mid-infrared opacity: a higher mass-loss rate makes a more opaque dust shell, which better shields molecules against photodissociation. However, parameters other than mass-loss, such as initial stellar masses and chemical abundances, probably also play an important role (Habing 1996).

A number of maser surveys have been carried out to measure stellar line-of-sight velocities toward the inner Galaxy, between 30° and -30° in longitude, (e.g. Baud et al. 1979; Blommaert et al. 1994; Lindqvist et al. 1992; Deguchi et al. 2000a,b; Sevenster et al. 1997a,b, 2001; Sjouwerman et al. 1998; Izumiura et al. 1999). These surveys mostly detected visually obscured OH/IR stars, i.e., AGB stars with 1612 MHz OH maser emission and high mass-loss rates.

Our survey of 86 GHz SiO maser emission towards infrared-selected Mira-like stars in the inner Galaxy, mostly at $b < 0.5^\circ$, (Messineo et al. 2002, hereafter Chapter II) led to the determination of 255 new line-of-sight velocities. The sample of targets (hereafter "SiO targets") was selected to be complementary to previous OH/IR surveys, so the sources with the reddest mid- and near-infrared colours were excluded.

In studying Galactic structure and kinematics it is important to combine the kinematic information and the stellar properties, such as luminosities, to explore any differences in the velocity fields of different tracers. In particular, it must be clarified whether OH/IR and SiO masing stars trace the same dynamic population, so that they can simply be combined to study the kinematics of the inner Galaxy.

The infrared photometry of our 441 SiO targets, derived from the large surveys DENIS (Epchtein et al. 1994), 2MASS (Cutri et al. 2003), ISOGAL (Omont et al. 2003; Schuller et al. 2003) and MSX (Egan et al. 1999; Price et al. 2001), was given by Messineo et al. (2004b, hereafter Chapter III). Corrections for interstellar extinction were discussed by Messineo et al. (2004a, hereafter Chapter IV). The present paper derives the bolometric magnitude of each target star, which we then compare with those of a sample of OH/IR stars.

Since most of the SiO targets are variable stars (Chapter III), their characterisation would require long-term, multi-frequency flux monitoring programs, which are not available yet. A first, although necessarily approximate discussion of their luminosities is possible even with single epoch observations, making use of the most recent infrared surveys.

The individual source numbers (e.g #99) are taken from Table 2 (86 GHz SiO

maser detections) and Table 3 (non-detections) of Chapter II.

5.2 Apparent bolometric magnitudes

The photometric measurements of each SiO target (Chapter IV) were corrected for interstellar extinction using the mean $K_{\rm S}$–band extinction found from the surrounding field stars. For the wavelength-dependence of the extinction, we assume a power law $A_\lambda/A_K = (\lambda/2.12\mu m)^{-1.9}$, so that for the individual bands we find effective band extinctions (A_I, A_J, A_H) = (6.78, 2.86, 1.66) $A_{\rm K_S}$. For the mid-infrared range we use the extinction law of Lutz (the extinction ratios are given in Table 2 of Chapter IV).

The bolometric stellar magnitudes, $m_{\rm bol}$, were computed by integrating over frequency ν using linear interpolations between the dereddened flux densities, $F_\nu(\nu)$. At the low frequency end we extrapolated to $F_{\nu=0} = 0$, and at the upper end we extrapolated the two highest frequency data–points, provided the flux decreases, to zero intensity. Loup et al. (2004) presented a comparison of different methods commonly used to compute bolometric magnitudes. Using model spectra of O-rich AGB stars (from Groenewegen & de Jong 1993), they showed that the integration method we adopt yields bolometric magnitudes which should on average be accurate within 0.3 mag. Since the DENIS I, J,$K_{\rm S}$ as well as the 2MASS J, H,$K_{\rm S}$ observations were each taken simultaneously, but both sets at different times, we computed the bolometric magnitudes separately using either the DENIS or 2MASS data. The SiO targets are mostly variable stars (Chapter III), so a comparison of both datasets yields some information on their average variability.

For all but two of the SiO target stars the low-frequency extrapolation is insignificant since it contains a negligible fraction of the total flux. Only for sources #76 and #347 the low-frequency extrapolation contributes more than 20% to the total integrated flux.

Given that usually $(K_{\rm S}-[15])_0 < 5$ mag, the main uncertainty in computing the bolometric magnitudes of the SiO target stars arises from the extrapolation at high frequencies. For 20 SiO targets a linear extrapolation was not possible because the flux density rises at high frequencies. For another 100 targets the blue extrapolation using 2MASS data or DENIS data contributes more than 20% to the bolometric flux.

For about half of our SiO stars (233 stars) we could compute bolometric magnitudes through a direct integration using either the DENIS or 2MASS data, with the flux in the extrapolated regions contributing less than 20% to the total. Unless otherwise stated, we adopt the average of these two integrations to attenuate the effect of variability.

For the other half of our sample, a bolometric magnitude could be integrated from only one dataset, since either the other data set is incomplete or the blue extrapolation is too uncertain in that the extrapolated spectral region contributes more than 20% to the total flux. For this half of the sample, when both the DENIS and 2MASS $K_{\rm S}$ measurements were available, we estimate bolometric magni-

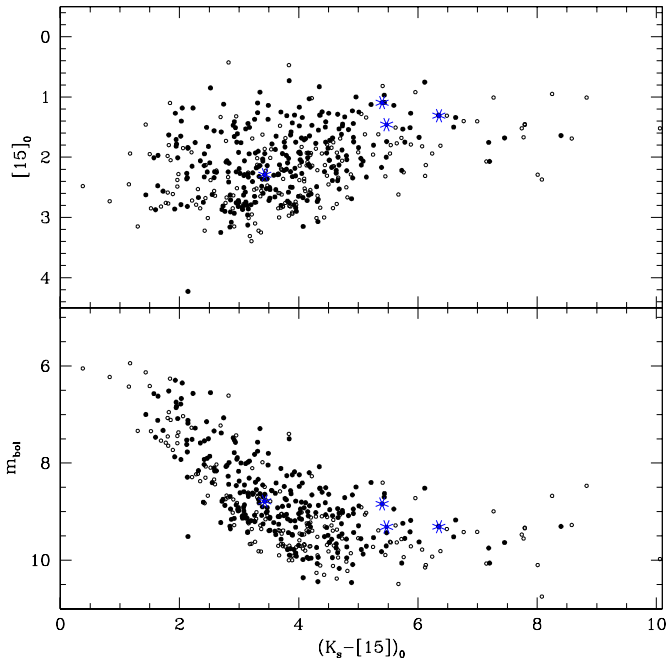

Figure 5.1: Lower panel: *Apparent bolometric magnitudes, $m_{\rm bol}$, versus $(K_{\rm S}-[15])_0$. Filled circles indicate objects with detected SiO maser emission, and open circles objects with no SiO detection. The four starred symbols show stars with observed OH emission (Chapter III). When both DENIS and 2MASS $K_{\rm S}$ measurements are available, or when both ISOGAL and MSX 15μm measurement are available, the average flux density is adopted.* **Upper panel:** *Apparent $[15]_0$ magnitudes versus the $(K_{\rm S}-[15])_0$ colour. Symbols are as in the lower panel.*

tudes using the bolometric corrections described in Appendix A and the average of the two $K_{\rm S}$–band flux densities. The average flux densities at 15 μm, when both ISOGAL and MSX 15μm measurement were available, was used.

The apparent bolometric magnitudes are plotted against the $(K_{\rm S}-[15])_0$ colour in Fig. 5.1. There is an misleading correlation because the range in $[15]_0$ is small compared with the range in $K_{\rm s0}$, and $m_{\rm bol}$ is dominated by the near-infrared flux.

There is a tail of stars at faint apparent bolometric magnitudes with a wider colour spread and redder $(K_{\rm S}-[15])_0$ colours (Fig. 5.1) (which is the consequence of selection of MSX sources, Chapter III). These redder colours are indicative of higher mass-loss rates.

5.2.1 Variability

Bolometric magnitudes of known Mira variables are found to vary up to 2 mag from minimum to maximum light (e.g. Whitelock et al. 1991, 2000).

Since we are using single epoch observations taken at random phase, the obtained bolometric magnitudes are also at a random phase.

Figure 5.2 shows that there is an rms scatter of ~ 0.35 mag between $m_{\rm bol}^{2MASS}$ and $m_{\rm bol}^{DENIS}$, which is mainly due to variability (Chapter III). There is a tight correlation between $m_{\rm bol}$ and $K_{\rm S}$ since both quantities are related by the bolometric correction $BC_{K_{\rm s}}$ (Appendix A). If we assume that all stars are sinusoidally variable with maximum-to-minimum amplitudes A_i, and that 2MASS and DENIS measurements are unrelated in time, then the rms of the amplitude distribution is equal to the rms of the differences between two measurements at random phase, i.e. 0.35 mag.

The observed scatter is only a lower limit to the stellar flux variability, because it only accounts for the near-infrared variation. However, since the dominant part of the stellar energy distribution of a Mira star is at near-infrared frequencies and since its pulsation amplitude decreases at lower frequencies, this variation is nearly that of the bolometric flux.

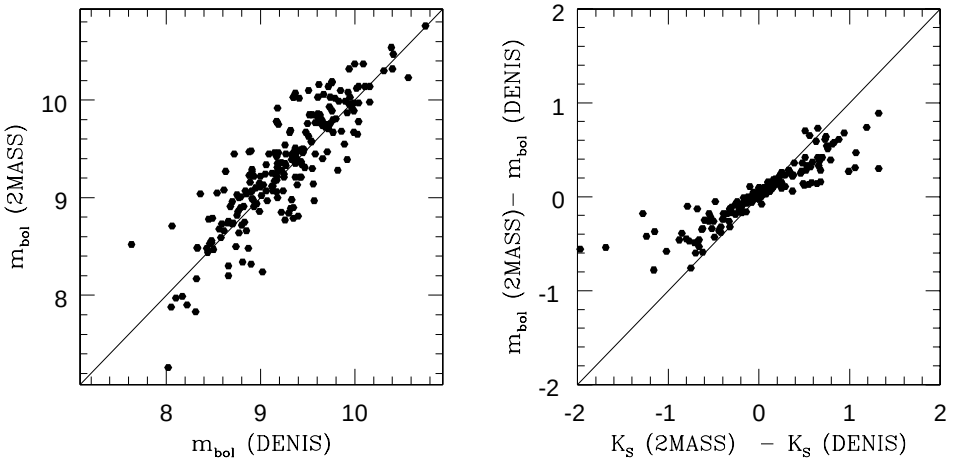

Figure 5.2: Left panel: *Apparent bolometric magnitudes derived using 2MASS data versus apparent bolometric magnitudes using DENIS data.* **Right panel:** *Differences in $m_{\rm bol}$ versus the corresponding differences between DENIS-$K_{\rm S}$ and 2MASS-$K_{\rm S}$.*

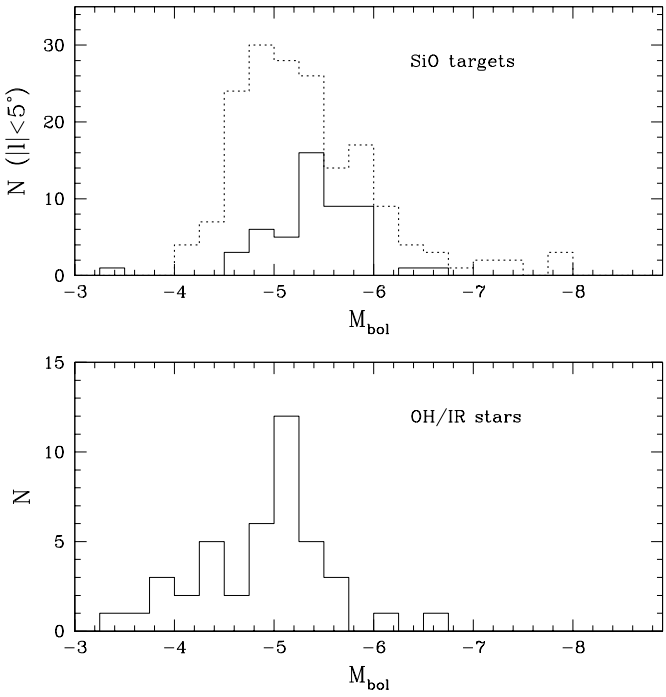

Figure 5.3: *Distribution of absolute bolometric magnitudes for an adopted distance of 8 kpc. SiO targets identified as possible foreground objects on the basis of their extinction (Chapter IV) are omitted from the plot.* **Upper panel:** *The dotted line shows the distribution of all SiO targets with $|l| < 5°$. The continuous line shows the distribution of SiO stars with ($A_{\rm K_S} > 2.0$ mag); most of them belong to the Nuclear Disk (see Sect. 5.6).* **Lower panel:** *For comparison the distribution of absolute magnitudes of a sample of OH/IR stars within 1° from the Galactic centre (Ortiz et al. 2002) is shown.*

5.3 SiO targets with $|l| < 5°$

5.3.1 Luminosities

We derive the "absolute" bolometric magnitudes, $M_{\rm bol}$, of 252 sources within the central 5° of the Galactic Centre adopting a distance of 8 kpc. Their "absolute" bolometric magnitudes, as shown in Fig. 5.3, ranges from -4 to -8 mag, with a peak around -5.0 mag. Our SiO targets appear to have mostly luminosities above that of the tip of the red giant branch at $M_{\rm bol} \sim -3.6$ (Ferraro et al. 2000), where the helium flash stops the ascent of the star on the red giant branch. This is typical for long period variable (LPV) stars in old metal-rich globular clusters.

Only two SiO targets (#77 and #347) have $M_{\rm bol}$ fainter than -4.0 mag; those stars could be in the early AGB phase or at a larger distance, or could have lower initial masses than the bulk of the SiO targets.

Another 33 (11%) of all SiO targets within 5 degrees from the Galactic Centre have $M_{\rm bol} < -6.5$ mag, and even brighter than -7.2 mag, which is the classical AGB limit (Iben & Renzini 1983). The maximum average luminosity observed for Galactic Mira stars corresponds to $M_{\rm bol}= -5.5$ mag (Glass et al. 1995; Olivier et al. 2001; Whitelock et al. 1991). Since the $K_{\rm S}$–band luminosity of a Mira star varies by up to about 2 magnitudes, for a single epoch measurement at random phase, we expect a distribution extending to $M_{\rm bol} = -6.5$ mag. The 33 targets brighter than this limit, could be either foreground stars, massive, young AGB stars, or evolved massive stars (red supergiants) (Nagata et al. 1993; Schuller 2002).

Near-infrared spectroscopy could reveal their true nature (e.g. Schultheis et al. 2003). By combining extinction information and luminosity Messineo et al. found that 20 of the 33 bright sources are likely to be foreground stars (Chapter IV). Their total extinction (interstellar plus circumstellar), which was calculated by assuming a photospheric colour for the central star, appears to be lower than the average interstellar extinction of stars in their respective surrounding fields.

We find five sources (#31, #75, #92, #128, #294) with $M_{\rm bol} < -7.2$ mag that cannot be explained as foreground on the basis of their extinction. One of them (#92) is classified as a possible red supergiant stars by Nagata et al. (1993). The bolometric magnitude given by Nagata et al. is in good agreement with our measurement. It is not unlikely that some of our other bright sources are also red supergiants.

5.3.2 Initial masses and ages

Estimates of the initial mass of pulsating AGB stars is problematic due to uncertainties in the pulsation mode, effective temperature (i.e., stellar radii), and of the mass-loss history (e.g. Marigo et al. 1996; Vassiliadis & Wood 1993). A degeneracy between age and metallicity further complicates the analysis of the distribution of stellar colours and luminosities (e.g. Frogel & Whitford 1987; van Loon et al. 2003; Whitelock et al. 1991).

The maximum luminosity reached at the end of the AGB phase strongly depends on the metallicity and initial mass of the star: a lower metallicity leads to a higher luminosity for a given initial mass.

Assuming solar metallicity and using the relation from Marigo et al. (1996) between the initial mass and maximum luminosity reached before the onset of the superwind (Renzini & Voli 1981; Vassiliadis & Wood 1993), we derive a distribution of initial masses for our SiO targets that ranges from 1.0 to 4.0 $\rm M_{\odot}$. This range is perhaps wider than the real due to the variability and our use of single epoch observations. For a solar metallicity, the majority of the SiO targets ($M_{\rm bol} = -4.5$ to -5.5) has ages ranging from 0.8 to 5 Gyr (Girardi et al. 2000). However, these are lower limits since stars with higher than the assumed solar metallicity would stay longer on the main sequence and would therefore be older when they reach the AGB.

A reliable empirical calibration of mass and age is possible only for Mira stars in globular clusters. Bulge Mira stars are more massive and/or metal rich than

Mira stars in Galactic globular clusters (e.g. Whitelock et al. 1991), as follows from their longer pulsation period (up to 800 days vs. 200-300 days in globular clusters) and higher luminosity. The most luminous AGB star in globular clusters has $M_{\rm bol} = -4.8$ mag (Guarnieri et al. 1997), while in the bulge they can reach -5.5 mag (Glass et al. 1995; Whitelock et al. 1991).

The presence of an intermediate age population ($2.2M_{\odot} <$ initial mass $< 8.0M_{\odot}$) in the inner Galaxy was suggested by, e.g., Cole & Weinberg (2002); van Loon et al. (2003). However, most of these studies are based on photometric observations of only giant stars. Because of differential reddening and the degeneracy between metallicity and age those studies could not securely confirm the presence of such a young population.

To infer the age of a stellar population it is crucial to detect the main-sequence turn-off. Using deep near-infrared photometry Zoccali et al. (2003) studied the stellar population of a bulge field at latitude $b = 6°$, from main–sequence stars to the AGB tip. They estimated an age of 10 Gyr for the field population and did not observe any other turn–off that could suggest the existence of an intermediate age population. Their number of luminous AGB stars agrees with that predicted for a population of that age. However, Zoccali's field is at $b = 6$ ° and it may not be representative of the in–plane population of the inner Galaxy.

Feltzing & Gilmore (2000) studied stars in the Baade's window field using visual HST data and also concluded that bulge stars are generally old, although the existence of a young and metal–rich population cannot be ruled out.

Evidence for a younger component comes from the distribution of OH/IR stars, in the central bulge that have a vertical scale height < 100 pc (Sevenster 1999b). They could belong to a distinct in–plane component. Furthermore, low latitude OH/IR stars stars and SiO targets do not trace the axisymmetric and old (8-10 Gyr) bulge population studied by Ng & Bertelli (1996), but the longitude–velocity diagram of maser stars shows evidence for a Galactic bar (Messineo et al. 2002; Sevenster 1999b). The masing population could be related to a more recent star formation event, e.g., triggered by the formation of the Galactic bar (e.g. Cole & Weinberg 2002; Sevenster 1999b; Sjouwerman et al. 1999).

New near–infrared photometric observations down to the main-sequence turn–off for inner Galactic fields at low latitude are important for improving our understanding of Galactic stellar population history, and can verify the possible existence of an intermediate age population.

Near–infrared spectroscopy would yield estimates of the metallicity of masing stars. The SiO targets, being bright at near–infrared wavelengths, are ideal targets for such a spectroscopic program.

5.3.3 Red Supergiant stars ?

Red supergiant stars are massive stars (> 9 M$_{\odot}$), which are burning helium (or carbon) in non-degenerate cores. They are often located in OB associations. The luminosity distribution of the SiO targets within 5° from the Galactic Centre,

shown in Fig. 5.3, suggests that a few red supergiant stars are also included, as supported by other indications described below.

IRAS counterparts of our SiO targets are mostly located in region IIIa of the IRAS two–colour diagram (Chapter III). Previous studies of IRAS sources have shown that most of the sources in region IIIa are O–rich AGB stars, but 26% may be red supergiant stars (Josselin et al. 1996; Winfrey et al. 1994).

Weak SiO maser emission is found in semiregular AGB and red supergiant stars (Alcolea et al. 1990), but red supergiants with large amplitudes are strong SiO emitters and their SiO maser intensity is comparable to that of Mira stars (Alcolea et al. 1990). The central star has an extended shell, generated by the strong pulsations as in LPVs, where the SiO maser activity takes place.

The line profile of the SiO masers normally has several components a few km s^{-1} wide over a range from 10 km s^{-1} (giant) to 20-40 km s^{-1} (supergiant) (Alcolea et al. 1999; Le Bertre & Nyman 1990). Our entire sample has an average SiO maser line width of 4.6 km s^{-1} with a scatter of 2.3 km s^{-1}. There are 12 sources with line width > 9 km s^{-1}: #31, #71, #87, #113, #117, #129, #135, #173, #190, #203, #223, #232. These spectra look similar to the broad and multiple peaked spectra typical of red supergiants (Cho et al. 1998; Haikala 1990). Seven of those 12 are located within 5° of the Galactic centre, and 4 (#31, #87, #113, #129) are also very luminous ($M_{\rm bol} < -6.5$ mag). The velocity–longitude distribution of bright ($M_{\rm bol} < -6.5$ mag) stars detected in our SiO maser survey appears distinct from that of the nuclear disk component or from bulge stars. The linear dependence of v and l suggests (see Sect. 5.7) that it is probably a Galactic disk component.

5.4 Comparison with OH/IR stars

For a comparison with our SiO targets, we also consider a sample of OH/IR stars (AGB stars with 1612 MHz OH maser emission) within 1° from the Galactic Centre (from Table 3 of Ortiz et al. 2002), a region fully mapped at 1612 MHz (Lindqvist et al. 1992; Sevenster et al. 1997a; Sjouwerman et al. 1998). Ortiz et al. found ISOGAL counterparts for all OH sources in ISOGAL fields, counterparts which are typically bright at 15 μm and have very red $(K_{\rm S}-[15])_0$ colours (reaching 12 mag; see upper panel of Fig. 5.4), which is indicative of high mass loss rates.

To directly compare luminosities of OH/IR stars with those of SiO targets, bolometric magnitudes must be calculated in the same way. We therefore calculated the interstellar extinction $A_{\rm K_S}$ toward each OH/IR star using 2MASS stars within 2′ from the position of the OH/IR star, following the procedure described in Chapter IV. Extinctions, $A_{\rm K_S}$, are found systematically larger (by up to 0.6 mag) than those adopted by Ortiz et al. (2002). This is due to our use of the (H, $K_{\rm S}$) data, which are less sensitive to extinction and therefore less affected by a low–extinction bias than (J, H) or (J, $K_{\rm S}$) data used by Ortiz et al. (2002). We adopted the near–infrared mean flux densities of the OH/IR stars given by Wood et al. (1998). When using Mathis' extinction law (for comparison with Ortiz et al. 2002)

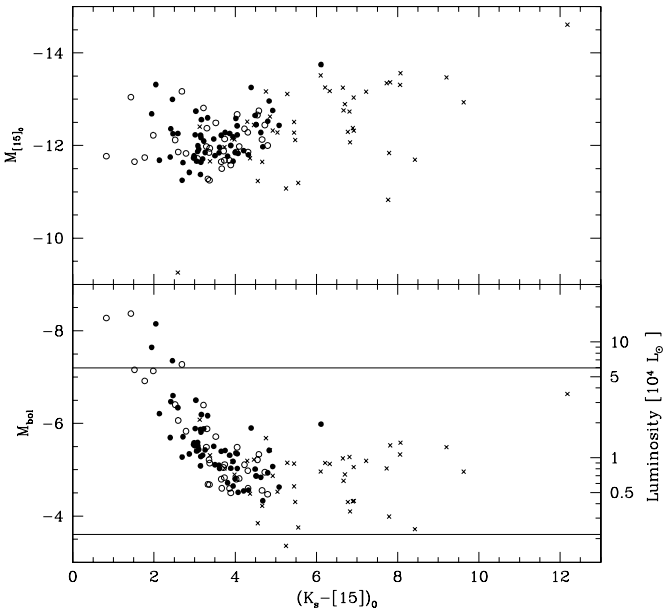

Figure 5.4: Lower panel: *"Absolute" bolometric magnitudes, M_{bol}, versus dereddened $(K_S-[15])_0$, adopting a distance of 8 kpc. When both DENIS and 2MASS K_S measurements, or both ISOGAL and MSX 15μm measurements are available, the average flux density is adopted. Circles show SiO targets from the ISOGAL fields of Ortiz et al. (2002), they cover about $\sim 0.84°$. Filled and open symbols indicate SiO maser detections and non–detections, respectively. For comparison, crosses show OH/IR stars within 1° from the Galactic Centre with a known period and ISOGAL counterpart (Ortiz et al. 2002). The line at $M_{\rm bol} = -3.6$ indicates the location of the tip of the red giant branch and the line at $M_{\rm bol} = -7.2$ the AGB limit.* **Upper panel:** *"Absolute" $[15]_0$ magnitudes, $M_{[15]}$, versus dereddened $(K_S-[15])_0$. Symbols are as in the lower panel.*

we obtained bolometric magnitudes consistent with those of Ortiz et al. (2002): since the spectral energy distribution of an OH/IR star peaks long-ward of 3μm (due to the presence of a thick circumstellar envelope), its bolometric magnitude is less sensitive to near–infrared interstellar extinction corrections than for SiO targets. However, when we adopt the mid–infrared extinction law suggested by Lutz et al. (as for the SiO targets, Chapter IV) we obtain bolometric magnitudes for the OH/IR stars brighter by up to 0.6 mag. Whenever a bolometric magnitude determination via direct integration (Sect. 5.2) was not possible, it was estimated using the bolometric correction described in the Appendix.

Figure 5.3 shows a comparison between the bolometric magnitude of our SiO targets (Sect. 5.2) with that of the OH/IR stars.

The peak of the OH/IR magnitude distribution is at ~ -5.1 mag, and translates

to an initial stellar mass of about 1.8 $M_{\odot}$ and an age of about 2 Gyr, using the models of Girardi et al. (2000) with solar metallicity. The peak for OH/IR stars appears consistent with the median of the bolometric magnitudes of SiO targets in the central 5°, although the distribution of the latter is broadened by variability and the use of single epoch observations.

For the 96 SiO targets (58 detections) from the same ISOGAL fields as the OH/IR stars of Ortiz et al. (2002), Fig. 5.4 shows the absolute bolometric magnitude of both OH/IR and SiO stars plotted against their $(K_{\rm S}-[15])_0$ colour. Distributions appear to differ in that SiO targets have bluer colours (due to our selection, Chapter III). This indicates that OH/IR stars have thicker envelopes due to higher mass–loss rates.

Note that here we are comparing only our SiO targets with known OH/IR stars. We imposed colour constraints for our target selection and we tried to be complementary to previous OH/IR studies by discarding the reddest mid- and near–infrared colour sources. It is quite well possible that there are SiO masing stars with colours much redder than what we considered, though according to Nyman et al. (1993) there should be a cut–off in the 86 GHz SiO maser intensity for very optically thick circumstellar envelopes.

In contrast to SiO targets, there are no OH/IR stars brighter than $M_{\rm bol} = -6.5$ (for a distance of 8 kpc) in our sample. The luminous SiO targets tend to be bluer than fainter ones, suggesting a thinner circumstellar envelope, which could also explain the lack of 1612 MHz OH maser line emission. Therefore, our sample includes luminous SiO masing AGB stars or red supergiants, with moderate mass–loss rates, not masing in OH. If the mass–loss rate increases with time (e.g. Lewis 1989) these objects could later also show 1612 MHz OH maser emission, which is more likely for thicker envelopes (Sevenster et al. 2001; Habing 1996).

In the chronological sequence of circumstellar masers presented by Lewis (1989), as first suggested by Bedijn (1987), circumstellar envelopes of AGB stars gradually evolve under slowly increasing rates of mass loss. Since the SiO masing shell is near the photosphere, the first maser emission to appear is that from SiO, while OH maser emission appears as the shell grows. The SiO maser emission is then the first to disappear when the mass loss declines.

The distributions of bolometric magnitudes of both SiO and OH/IR stars, as seen in Fig. 5.3, peak at about the same value, which suggests that both populations trace the same epoch of star formation, but SiO masing stars have less evolved circumstellar envelopes (see also Chapter III). This is supported also by the different distribution of SiO and OH/IR stars in the period–luminosity diagram (Sect. 5.5).

5.5 Period–Luminosity relation

Our SiO targets include 15 LPVs from the sample of Glass et al. (2001), Chapter II. Figure 5.5 plots their bolometric magnitudes against their periods, showing that they fall above the period–luminosity distribution of Mira stars in the Sgr–I field

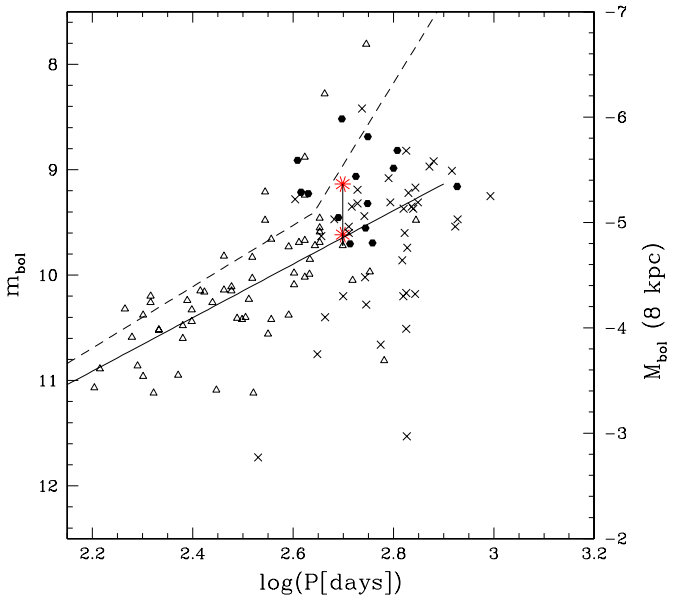

Figure 5.5: *The period–luminosity relation of LPV stars. Dots represent 15 LPV stars in our SiO maser sample located within 24′ from the Galactic Centre (Glass et al. 2001). They have a bright ISOGAL counterpart, but no known OH maser emission. Triangles show Mira stars located in the Sgr–I field (Glass et al. 1995), for which we plot the mean bolometric magnitudes. For #153, the only SiO target located in the Sgr–I field, we plot both magnitudes (stars) obtained using DENIS and 2MASS data, and connect them to the mean $m_{\rm bol}$ value found by Glass et al. (1995) with a vertical line. Crosses show OH/IR stars with ISOGAL counterpart (Ortiz et al. 2002). The continuous line represents the relationship found by Glass et al. (1995), while the dashed line is a fit for LMC Mira stars (Hughes & Wood 1990), assuming a distance modulus of 18.55 mag for the LMC and 14.5 mag for the Galactic Centre.*

(Glass et al. 1995). However, in the Sgr–I field Mira stars with period longer than 450 days are rare. Our SiO stars may support a steepening of the period–luminosity relation for period longer than 450 days, as observed in the Magellanic Clouds (Hughes & Wood 1990).

The standard deviation in the period–luminosity relation of Mira stars in Sgr–I is 0.36 mag (Glass et al. 1995), which partly arises from the spread in distance, and partly from the uncertainty in the apparent bolometric magnitude. A spread of ± 2 kpc in distance at a distance of 8 kpc causes a spread in $M_{\rm bol}$ of ± 0.55 mag. Bolometric magnitudes given by Glass et al. (1995) were obtained adopting the mean values of monitored infrared flux densities. The period–luminosity relation obtained using mean magnitudes of Mira stars in the Magellanic Clouds is less sensitive to distance uncertainties, resulting in a scatter of only 0.15 mag (Feast

et al. 1989).

Our sample has one SiO star located in the Sgr–I field, #153. Its $m_{\rm bol}$ calculated using DENIS data is 9.62 mag, identical to the mean value obtained by Glass et al. (2001). When using 2MASS data we find $m_{\rm bol} = 9.14$ mag. Considering the pulsation amplitude $\Delta K = 1.38$ mag (Glass et al. 1995), both measurements are consistent.

The 15 LPV/SiO targets in the Galactic Centre from Glass et al. (2001) suffer from strong extinction ($A_{\rm Ks} > 2$ mag) and using the kinematic information for the 11 which were detected in our SiO maser survey, we conclude that they are members of the central nuclear disk (see Sect. 5.6). They are therefore at about the distance of the Galactic centre. Assuming an isotropic distribution of stars in the nuclear disk, a range of longitudes of $\pm 1.5^\circ$ translates to a distance range of ± 200 pc, and a corresponding distance modulus range of ± 0.05 mag. Their dispersion on the period–luminosity plane is mostly due to the uncertainty in the bolometric magnitude ($\sim$0.35 mag, see Sect. 5.2) and in the extinction (Chapter IV).

Since we selected bright ISOGAL and MSX sources (Chapter II) and since mid–infrared flux density correlates with period (see the 12μm period–luminosity relation in Whitelock et al. 1991), it is not surprising that the LPVs we observed have periods above 400 days (Fig. 5.5). Imai et al. (2002) searched for SiO maser emission toward the entire sample of Mira stars near the Galactic centre detected in K–band by Glass et al. (2001) and confirmed the expected increase of the detection rate with increasing period. While for periods below 300 days the SiO maser detection rate is below 20%, above 400 days it rises to 60% . OH/IR stars also have typical periods above 400 days (Fig. 5.5). Thereby, SiO and OH maser emission mainly trace long period AGB variables.

Unlike Mira stars, OH/IR stars do not follow a period–luminosity relation in the Galactic Centre region (Ortiz et al. 2002, and references therein). Most of them for a given magnitude have a longer period than that predicted by the Mira period–luminosity relation, so OH/IR stars and SiO targets are differently distributed.

Pulsation models predict that due to a dramatic increase of the mass loss rate (superwind phase), a Mira star significantly stretches its pulsation period, while its luminosity remains almost constant (Vassiliadis & Wood 1993), and becomes an OH/IR star. OH/IR stars have then longer periods for a given luminosity than those found in Mira stars.

5.6 Stars in the the Nuclear Disk and a fourth dimension: extinction

The line of sight extinction is a useful fourth dimension along with position (l, b) and velocity to characterise various Galactic components.

Around zero longitude our stellar longitude–velocity ($l - v$) diagram reveals a stellar nuclear disk, which follows the high velocity gaseous **nuclear disk** (e.g. Binney et al. 1991; Burton & Liszt 1978).

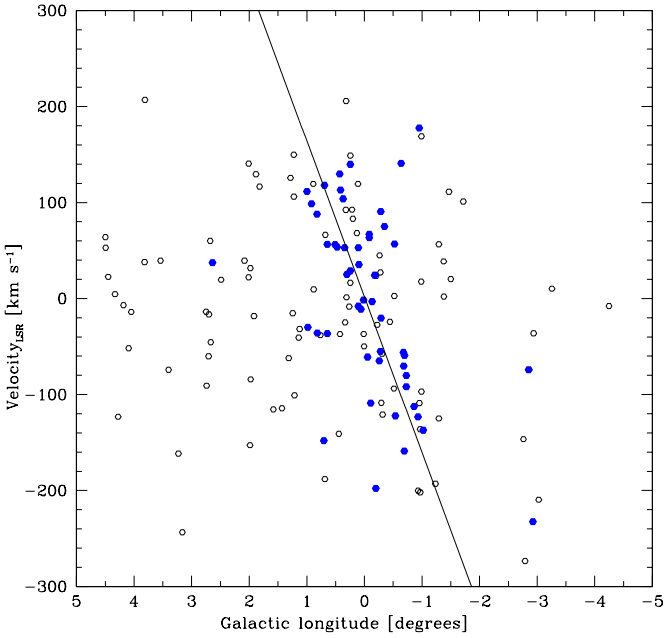

Figure 5.6: *Stellar longitude–velocity diagram of our 86 GHz SiO masers. Filled circles indicate sources with interstellar extinction $A_{\rm K_S}$ above 2 mag. Most of these belong to the fast rotating nuclear disk. The continuous line indicates our best fit to the nuclear disk component.*

There is a unique correspondence between interstellar extinction and velocity. When we select SiO targets at interstellar extinction $A_{\rm K_S} > 2$ mag (Fig. 5.6), we find that most of these stars kinematically trace the nuclear disk. Their line–of–sight velocities range from $\sim +150$ to ~ -200 km s^{-1}, similar to the gaseous nuclear disk line–of–sight velocities (cf. the ^{13}CO ($l - v$) diagram in Fig. 4 of Bally et al. 1988). Therefore, the extinction enables us to identify individual stars belonging to the nuclear disk.

The stellar nuclear disk rotates rapidly around the Galactic Centre: our best–fit yields a gradient of $162(\pm 40)$ km s^{-1} per degree longitude. This slope is consistent with a value of $180(\pm 15)$ km s^{-1} found for OH/IR stars with high circumstellar expansion velocity located within 1° of the the Galactic Centre (Lindqvist et al. 1992).

To investigate whether the 56 SiO targets with $A_{\rm K_S} > 2$ mag also show distinct physical properties, their bolometric magnitude distribution is shown in Fig. 5.3. The distribution peaks at -5.4 mag, a peak slightly more luminous than the average luminosity of SiO targets within 5°. However, their luminosity is consistent with those of variable AGB stars. There is only one SiO target with $M_{\rm bol} < -6.5$ mag, #99, which may be a young star. Its location ($l = 0.8^\circ$; $v = -36.0$ km s^{-1}; 2σ

away from our best fit) indicates that it is probably unrelated to the nuclear disk in origin and kinematics.

The 11 LPVs from Glass et al. (2001) that we detected at 86 GHz (see also Sect. 5.5) all belong to the nuclear disk population, as their positions ($|l| < 1.5, |b| < 0.5$), their interstellar extinctions ($A_{\rm K_S} > 2.0$ mag) and their line–of–sight velocities confirm.

5.7 Bolometric magnitudes and the $l - v$ diagram

Different Galactic components give a different signature in the $(l - v)$ diagram. However, a stellar $(l - v)$ diagram alone is not sufficient to locate individual stellar components, mainly due to the velocity dispersion of the stars, that smooths various features. The inclusion of additional distance information will notably improve the understanding of the $(l - v)$ diagram. The stellar bolometric magnitude may serve as a first approximation of distance.

In section 5.3, we have already noticed the presence of a group of stars brighter than the typical luminosity of a Mira star at its maximum ($M_{\rm bol} = -6.5$ mag) when we assume a distance of 8 kpc. In Figure 5.7 we illustrate the $l - v$ diagram of SiO targets with $M_{\rm bol}$ fainter and brighter than -6.5 mag. The bright sample appears to be distributed differently from the faint sample, since it has a low velocity dispersion (~ 30 km s^{-1}), independently of longitude. The stars that were classified as foreground stars on the basis of extinction consideration (crosses in Fig. 5.7; see also Chapter IV), almost all belong to the bright group. This indicates that the bright stars are closer on average to the Sun than fainter ones and that their luminosities are overestimated by assuming the distance of the Galactic centre. But then how nearby are those stars? Do they trace a specific Galactic component?

An estimate of their distance can be inferred by assuming circular orbits. However, this assumption clearly does not hold for the central kiloparsecs, due to both the presence of a bar and the fact that bulge stars might have a velocity dispersion larger than the rotation velocity. Hence, we calculated Galactocentric distances, under the assumption of circular orbits, for SiO targets at longitudes $> 10^\circ$. We adopted the relation between the longitude, radial velocity and distance (Burton 1988):

$$v = R_\odot [\frac{V(R)}{R} - \frac{V(R_\odot)}{R_\odot}] \sin(l), \tag{5.1}$$

where $V(R)$ is the circular rotation velocity at Galactocentric distance R, the Galactocentric distance of the Sun is taken to be $R_\odot = 8.0$ kpc, and the circular velocity of the Sun $V(R_\odot) = 200$ km s^{-1}. Adopting $V(R) = V(R_\odot)(R/R_\odot)^{0.1}$ km s^{-1} (Binney et al. 1991), and inverting equation (1), it follows that:

$$R = \frac{8.0}{(1 + \frac{v}{(200 \times \sin(l)}))^{1.11}} (\text{in kpc}), \tag{5.2}$$

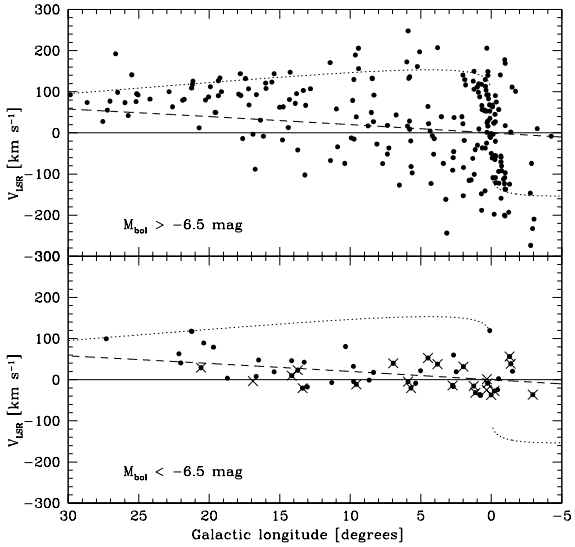

Figure 5.7: *Longitude–velocity diagram of SiO targets.* **Upper panel:** *SiO targets with $M_{\rm bol} > -6.5$ mag (assuming a distance modulus for the Galactic centre of 14.5 mag). The dotted line shows the curve defined by the line-of-sight velocities of tangent points to circular orbits, as predicted by Eq. 5.1. The dashed line indicates a circular orbit at a galactocentric distance of 5 kpc.* **Bottom panel:** *Dots indicate SiO targets with $M_{\rm bol} < -6.5$ mag. Crosses indicate SiO targets classified as foreground on the basis of extinction (Chapter IV).*

Bright sources are found to have an almost homogeneous distribution in Galactocentric distance, from 0 to 15 kpc. Fainter stars (Fig. 5.8) peak at about 3 kpc from the Galactic centre, i.e. at about the corotation radius of ~ 3.4 kpc (e.g. Englmaier & Gerhard 1999).

Since interstellar extinction increases with distance, another independent way to estimate distances is to use a model of dust distribution in the inner Galaxy. Using the implementation of Drimmel et al. (2003) based on COBE/DIRBE data, we calculated for each line of sight toward a SiO target the interstellar extinction as a function of distance. By interpolating the models at the values of derived interstellar extinction (Chapter IV), we have estimated distances to each SiO target.

The model of Drimmel et al. does not include the nuclear disk molecular complex and therefore it fails in reproducing the distance of nuclear disk stars. It predicts that all SiO targets are within a Galactocentric distance of 5 kpc and confirms a peak around corotation.

We used two independent methods to estimate distances, one based on kinematics and another based on extinction. Although the uncertainty are large (see right panel of Fig. 5.8), from both methods we find that most of SiO targets have a Galactocentric distance within 5 kpc, with a peak around corotation. The bright

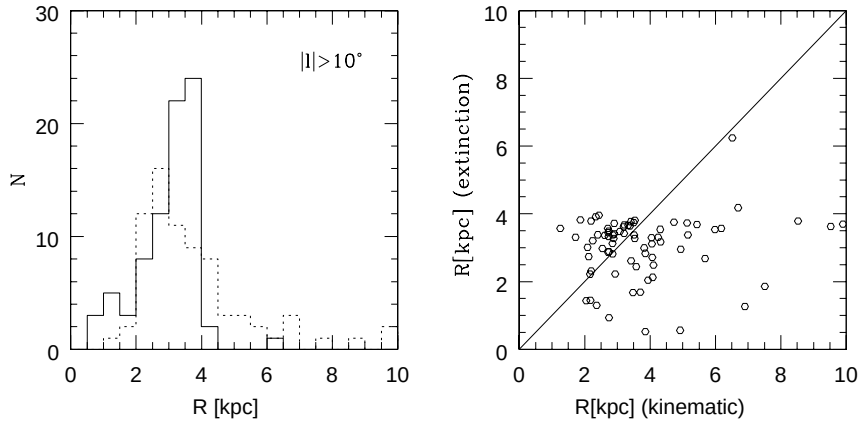

Figure 5.8: Left side*:The continuous histogram shows the distribution of Galactocentric distances inferred for SiO targets at longitudes $l > 10^\circ$ using interstellar extinction estimates towards the line of sight of each SiO target and a model of Galactic dust distribution (Drimmel et al. 2003). The dotted histogram shows the distribution of Galactocentric distances inferred for SiO targets at longitudes $l > 10^\circ$ assuming circular orbits.* **Right side***: Distance estimates from interstellar extinction versus kinematic distances.*

stars, however, do not seem confined at a specific Galactocentric distance.

It is difficult to argue about the nature of each single SiO target. The difference in distance modulus of a star at the Galactic centre and at a Galactocentric distance of 5 kpc is 2.1 mag, thus we might have overestimated the luminosity of the SiO target stars. The true luminosity of the "bright" stars could be below the AGB limit ($M_{\rm bol} < -7.2$ mag) and therefore they could be all AGB stars, rather than red supergiants. However, the luminosity range of these two classes of stars overlaps, and some of them could still be red supergiants as the SiO maser line widths and the low velocity dispersion suggest. Near–infrared spectroscopy is needed to distinguish between AGB and red supergiants. Furthermore, a near-infrared monitoring program would provide pulsation periods and therefore another independent estimate of the distance of each SiO target.

We are currently working on a kinematic study of the SiO targets based on a more realistic Galactic gravitational potential, which will be presented in a forthcoming paper.

5.8 Conclusion

Bolometric magnitudes for SiO target stars were computed from available flux density measurements. Adopting a distance of 8 kpc for all stars within 5° from the Galactic Centre we find a peak in the luminosity distribution at $\rm M_{bol} = -5.1$ mag, which coincides with the peak shown by OH/IR stars in the Galactic Centre

(e.g. Ortiz et al. 2002). Assuming a solar metallicity this peak magnitude corresponds to stars with an initial mass of 1.8 $M_\odot$ and an age of about 2 Gyr.

Our sample includes 15 LPVs from the sample of Glass et al. (2001). We found that these fall above the period–luminosity relation found by Glass et al. (1995), thus differing from OH/IR stars. This supports a chronological sequence for circumstellar masers proposed by Lewis (1989). We also find evidence for a steepening of the bulge period–luminosity relation for periods larger than 450 days, as found for Magellanic Cloud LPVs.

In contrast to OH/IR stars (Ortiz et al. 2002), SiO targets contain a significant fraction (11%) of blue and luminous stars ($M_{\rm bol} < -6.5$ mag). These stars are most likely massive AGB stars, or red supergiant stars, foreground with respect to the bulge. Their longitude–velocity distribution has a low velocity dispersion, which identifies a component, distinct from the bulge, perhaps related to the disk or to the molecular ring. A full dynamical analysis of SiO stars will be presented in a subsequent paper.

We found a unique relation between interstellar extinction and kinematic properties of SiO stars. Those with $A_{\rm K_S} > 2.0$ mag belong to the stellar Nuclear Disk.

Acknowledgements. We thank C. Loup and M.–R. Cioni for making their work on bolometric magnitudes available prior publication. MM is grateful to J. Meisner for help with statistical computations and to Glenn van de Ven for his enthusiastic and great discussions on stellar dynamics. The DENIS project was carried out in the context of EARA, the European Association for Research in Astronomy. This publication makes use of data products from the IRAS data base server, from the Two Micron All Sky Survey, from the Midcourse Space Experiment, and from the SIMBAD data base. The work of MM is funded by the Netherlands Research School for Astronomy (NOVA) through a *netwerk 2, Ph.D. stipend*.

Appendix A: Bolometric corrections

The bolometric correction for a given photometric band is defined as $BC_\lambda = m_{\rm bol} - m_\lambda$. Bolometric corrections for late–type stars as a function of spectral type or colour are used to derive stellar luminosities. However, there are uncertainties in their estimates and applicability. Stars of different temperature, metallicity and mass–loss rate have a different energy distribution and therefore a different bolometric corrections. Variability is also a complication for a proper determination of the bolometric correction. Long period variables are characterised by extended atmospheres and their energy distribution differs from other static late–type giants because of water absorption seen from the J–band to the L–band (Frogel & Whitford 1987; Matsuura et al. 2002). The amount of absorption varies from star to star and with stellar phase. At the present time there are a number of already completed near–infrared monitoring programs of large amplitude AGB stars, in the solar neighbourhood, in the South Galactic Cap and in the Magellanic Clouds, which provide accurate average bolometric magnitudes of oxygen–rich large amplitude variables (Olivier et al. 2001; Whitelock et al. 2000, 1994, 2003). We use

these data to derive various bolometric corrections for these type of objects and compare these with results for stars in the inner Galaxy.

A.1 Bolometric corrections of monitored LPV stars

In order to have a large sample of LPV stars, well studied and covering a wide range of colours, we assembled photometric catalogues of LPV stars from Olivier et al. (2001) and Whitelock et al. (2000, 1994, 2003). All near–infrared magnitudes are in the SAAO system (Carter 1990). Stellar fluxes are corrected for reddening only in the work of Olivier et al. (2001). However, the effect of interstellar extinction is negligible because these stars are nearby or outside of the Galactic plane, and because the bulk of their energy is emitted at infrared wavelengths. Bolometric magnitudes are reported by the authors and, with the exception of the Hipparcos sample, were derived for each star by integrating under a spline curve fitted to the mean near–infrared ($JHKL$) flux densities and the IRAS 12 and 25 μm flux densities as a function of frequency, and using two extrapolations for longer and shorter wavelengths as described in Whitelock et al. (1994). For the sample of low mass–loss Mira stars observed by Hipparcos (Whitelock et al. 2000) bolometric magnitudes were calculated by fitting blackbody curves to the ($JHKL$) flux densities as a function of frequency. The blackbody fitting is a good approximation of these low mass–loss stars and for them blackbody and spline–fit bolometric magnitudes agree to better than 0.2 mag (Whitelock et al. 2003). Figure A.1 shows various bolometric corrections versus colours. The IRAS 12 μm magnitude, [12], is obtained adopting a zero point of 28.3 Jy (Beichman et al. 1988). BC_K is well correlated with $K-[12]$ rather than $J-K$. The least–squares polynomial fits to the bolometric correction BC_K and $BC_{[12]}$, which give a good match to the data ($\sigma = 0.08$ mag) over the range $1.0 < (K-[12]) < 7.0$, shown by the continuous lines in Fig. A.1, are given by:

$$BC_K = 2.219 + 0.7351(K-[12]) - 0.1299(K-[12])^2$$

$$BC_{[12]} = 2.219 + 1.735(K-[12]) - 0.1299(K-[12])^2.$$

These two curves are complementary to each other. Practically for $K-[12]$ smaller than 4 mag it is better to use BC_K due to the flatness of the curve. For $K-[12]$ redder than 4 mag BC_K decreases steeply with increasing colour, while $BC_{[12]}$ is more stable. The narrowness of (BC_K,$K-[12]$) and ($BC_{[12]}$, $K-[12]$) sequences also suggests that they do not depend on metallicity; in fact, the Magellanic Clouds objects also follow the same relation. Instead, the (BC_K, $J-K$) sequence depends on metallicity as found by Frogel & Whitford (e.g. 1987) comparing local stars and bulge stars.

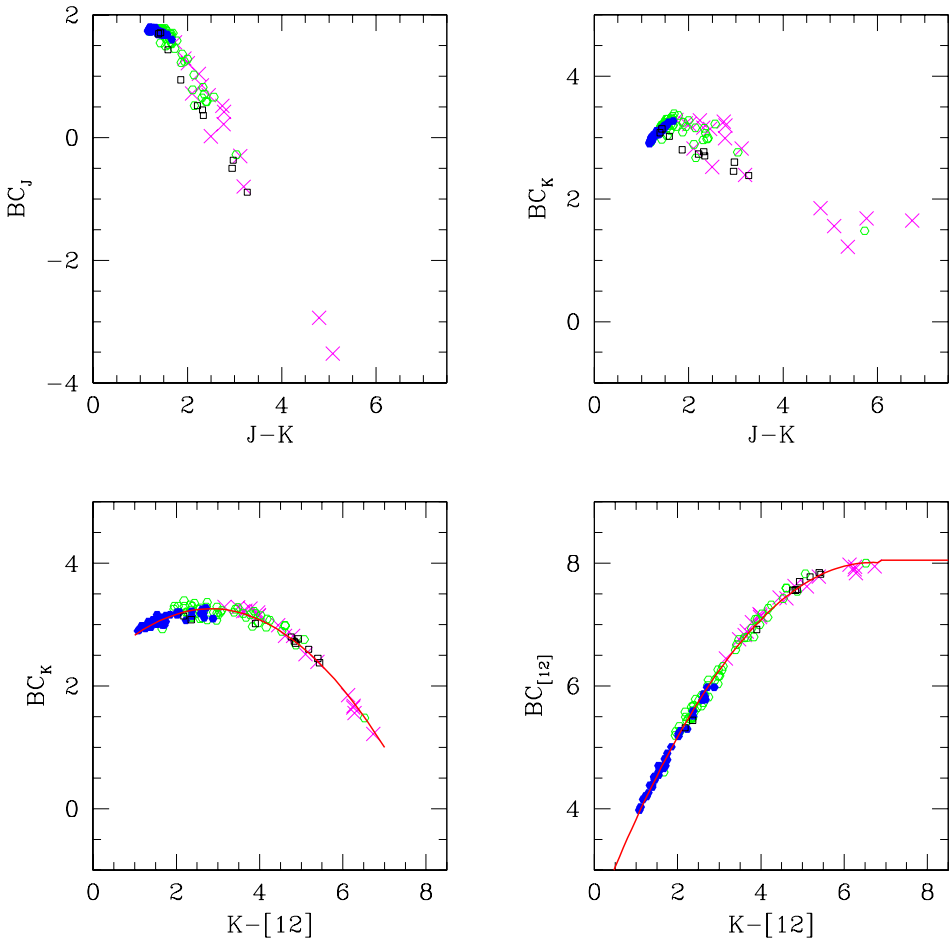

Figure A.1: *Monitored LPV stars - Bolometric corrections as a function of various colours. Filled circles represent LPV stars in the solar vicinity detected by Hipparcos (Whitelock et al. 2000); open circles represent LPV stars in the Southern Galactic Cap (Whitelock et al. 1994); crosses indicate local high mass–loss LPV stars (Olivier et al. 2001); squares represent obscured LPV stars in the Large Magellanic Cloud (Whitelock et al. 2003). The IRAS 12μm magnitude is defined as* $[12] = -2.5 \log F_{12}[\mathrm{Jy}]/28.3$.

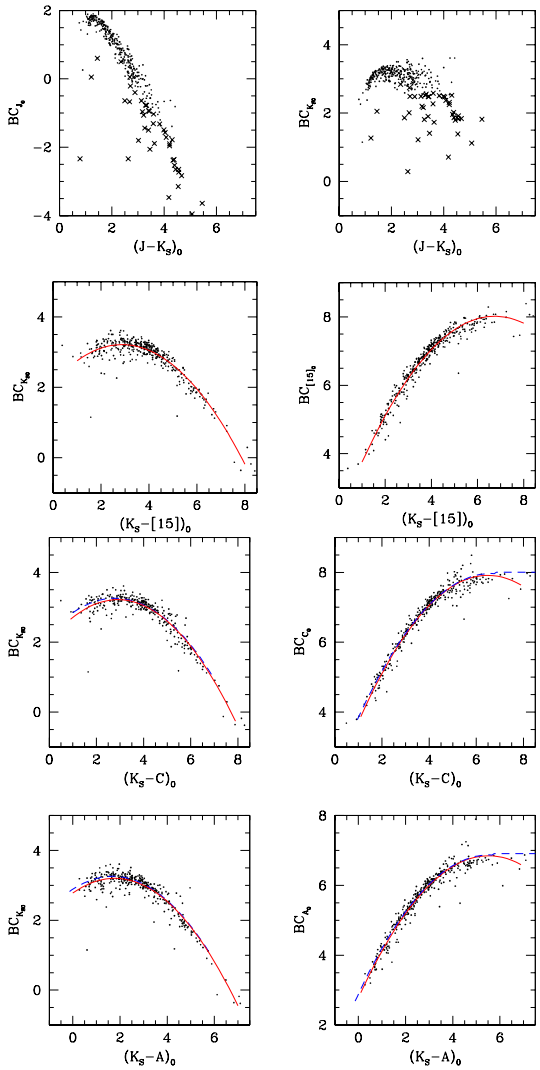

Figure A.2: *SiO targets - Bolometric corrections versus colours. Crosses are sources with* $(K_S - [15])_0$ *redder than 5 mag. Only sources with bolometric magnitudes well determined are plotted, i.e. when the extrapolation to shorter wavelengths has a negligible contribute to the integrated bolometric magnitude* ($< 20\%$)*. The 2MASS dataset is plotted. DENIS data are plotted only for sources with poor 2MASS photometry. When both ISOGAL and MSX 15*μ*m measurement are available, then the average flux density is adopted. Continuous lines indicate our best fits. Dashed lines show the relation found for monitored LPV stars, adapted using the equation* $A - [12] = 1.15, C - [12] = 0.05$ *mag (Chapter IV).*

A.2 Bolometric corrections for stars in the inner Galaxy

For the SiO targets we derived bolometric magnitudes as described in Sect. 5.2. Bolometric corrections for the $K_{\rm S}$ and 15 μm band are computed from the $m_{\rm bol}$ and plotted against the dereddened $(K_{\rm S}-[15])_0$ colour in Fig. A.2. Identical results are found using separately 2MASS $m_{\rm bol}$ and $K_{\rm S}$ or DENIS $m_{\rm bol}$ and $K_{\rm S}$ and/or ISOGAL [15] or MSX D (15μm) band magnitudes. The plotted continuous line is a least–squares polynomial fit, which gives a good match to the data ($\sigma = 0.25$ mag) over the range $1.0 < (K_{\rm S}-D)_0 < 8.0$:

$$BC_{K_{\rm s}} = 2.138 + 0.745(K_{\rm s} - [15])_0 - 0.1294(K_{\rm s} - [15])_0{}^2.$$

Analogously, using the MSX A (8μm) band, the following fit is obtained as a function of $(K_{\rm S}-A)_0$ colour in the range $0.0 < (K_{\rm S}-A)_0 > 7.0$ ($\sigma = 0.25$ mag):

$$BC_{K_{\rm s}} = 2.780 + 0.475(K_{\rm s} - A)_0 - 0.1337(K_{\rm s} - A)_0{}^2.$$

Eventually, using the MSX C (12μm) band, the following fit is obtained as a function of $(K_{\rm S}-C)_0$ colour in the range $1.0 < (K_{\rm S}-C)_0 < 8.0$ ($\sigma = 0.25$ mag):

$$BC_{K_{\rm s}} = 2.037 + 0.813(K_{\rm s} - C)_0 - 0.1398(K_{\rm s} - C)_0{}^2.$$

The fit to our SiO targets for $(K_{\rm S}-C)_0 < 2$ mag gives a bolometric correction $BC_{K_{S_0}}$ smaller (up to 0.1 mag) than those derived for Hipparcos Mira stars, which have a similar $(K - [12])$ colour. However, within the uncertainty of the fits the two curves derived are consistent.

References

Alcolea, J., Bujarrabal, V., & Gomez-Gonzalez, J. 1990, A&A, 231, 431

Alcolea, J., Pardo, J. R., Bujarrabal, V., et al. 1999, A&AS, 139, 461

Bally, J., Stark, A. A., Wilson, R. W., & Henkel, C. 1988, ApJ, 324, 223

Baud, B., Habing, H. J., Matthews, H. E., & Winnberg, A. 1979, A&AS, 35, 179

Bedijn, P. J. 1987, A&A, 186, 136

Beichman, C. A., Neugebauer, G., Habing, H. J., Clegg, P. E., & Chester, T. J. 1988, in NASA RP-1190, Vol. 1 (1988)

Binney, J., Gerhard, O. E., Stark, A. A., Bally, J., & Uchida, K. I. 1991, MNRAS, 252, 210

Blitz, L. & Spergel, D. N. 1991, ApJ, 379, 631

Blommaert, J. A. D. L., van Langevelde, H. J., & Michiels, W. F. P. 1994, A&A, 287, 479

Burton, W. B. 1988, in Galactic and Extragalactic Radio Astronomy, 295–358

Burton, W. B. & Liszt, H. S. 1978, ApJ, 225, 815

Carter, B. S. 1990, MNRAS, 242, 1

Cho, S., Chung, H., Kim, H., et al. 1998, ApJS, 115, 277
Cole, A. A. & Weinberg, M. D. 2002, ApJ, 574, L43
Cutri, C. M., Skrutskie, M. F., & Van Dyk, S. 2003, avalaible on line at `http://www.ipac.caltech.edu/2mass/`
de Vaucouleurs, G. 1964, in IAU Symp. 20: The Galaxy and the Magellanic Clouds, 195
Deguchi, S., Fujii, T., Izumiura, H., et al. 2000a, ApJS, 130, 351
—. 2000b, ApJS, 128, 571
Drimmel, R., Cabrera-Lavers, A., & López-Corredoira, M. 2003, A&A, 409, 205
Egan, M. P., Price, S. D., Moshir, M. M., et al. 1999, AFRL-VS-TR-1999, 1522
Englmaier, P. & Gerhard, O. 1999, MNRAS, 304, 512
Epchtein, N., de Batz, B., Copet, E., et al. 1994, Ap&SS, 217, 3
Feast, M. W., Glass, I. S., Whitelock, P. A., & Catchpole, R. M. 1989, MNRAS, 241, 375
Feltzing, S. & Gilmore, G. 2000, A&A, 355, 949
Ferraro, F. R., Montegriffo, P., Origlia, L., & Fusi Pecci, F. 2000, AJ, 119, 1282
Frogel, J. A. & Whitford, A. E. 1987, ApJ, 320, 199
Girardi, L., Bressan, A., Bertelli, G., & Chiosi, C. 2000, A&AS, 141, 371
Glass, I. S., Matsumoto, S., Carter, B. S., & Sekiguchi, K. 2001, MNRAS, 321, 77
Glass, I. S., Whitelock, P. A., Catchpole, R. M., & Feast, M. W. 1995, MNRAS, 273, 383
Groenewegen, M. A. T. & de Jong, T. 1993, A&A, 267, 410
Guarnieri, M. D., Renzini, A., & Ortolani, S. 1997, ApJ, 477, L21
Habing, H. J. 1996, A&A Rev., 7, 97
Haikala, L. K. 1990, A&AS, 85, 875
Hughes, S. M. G. & Wood, P. R. 1990, AJ, 99, 784
Iben, I. & Renzini, A. 1983, ARA&A, 21, 271
Imai, H., Deguchi, S., Fujii, T., et al. 2002, PASJ, 54, L19
Izumiura, H., Deguchi, S., Fujii, T., et al. 1999, ApJS, 125, 257
Josselin, E., Loup, C., Omont, A., Barnbaum, C., & Nyman, L.-A. 1996, A&A, 315, L23
Le Bertre, T. & Nyman, L.-A. 1990, A&A, 233, 477
Lewis, B. M. 1989, ApJ, 338, 234
Lindqvist, M., Winnberg, A., Habing, H. J., & Matthews, H. E. 1992, A&AS, 92, 43
Loup, C., Groenewegen, M. A. T., Cioni, M. R., et al. 2004, in preparation
Marigo, P., Bressan, A., & Chiosi, C. 1996, A&A, 313, 545
Matsuura, M., Yamamura, I., Cami, J., Onaka, T., & Murakami, H. 2002, A&A, 383, 972
Messineo, M., Habing, H. J., Menten, K. M., Omont, A., & Sjouwerman, L. O. 2004a, A&A (Chapter IV)
—. 2004b, A&A, 418, 103 (Chapter III)

Messineo, M., Habing, H. J., Sjouwerman, L. O., Omont, A., & Menten, K. M. 2002, A&A, 393, 115 (Chapter II)

Nagata, T., Hyland, A. R., Straw, S. M., Sato, S., & Kawara, K. 1993, ApJ, 406, 501

Nakada, Y., Onaka, T., Yamamura, I., et al. 1991, Nature, 353, 140

Ng, Y. K. & Bertelli, G. 1996, A&A, 315, 116

Nyman, L.-A., Hall, P. J., & Le Bertre, T. 1993, A&A, 280, 551

Olivier, E. A., Whitelock, P., & Marang, F. 2001, MNRAS, 326, 490

Omont, A., Gilmore, G. F., Alard, C., et al. 2003, A&A, 403, 975

Ortiz, R., Blommaert, J. A. D. L., Copet, E., et al. 2002, A&A, 388, 279

Price, S. D., Egan, M. P., Carey, S. J., Mizuno, D. R., & Kuchar, T. A. 2001, AJ, 121, 2819

Renzini, A. & Voli, M. 1981, A&A, 94, 175

Schuller, F. 2002, PhD Thesis: Université Pierre et Marie Curie, Paris 6.

Schuller, F., Ganesh, S., Messineo, M., et al. 2003, A&A, 403, 955

Schultheis, M., Lançon, A., Omont, A., Schuller, F., & Ojha, D. K. 2003, A&A, 405, 531

Sevenster, M. N. 1999, MNRAS, 310, 629

Sevenster, M. N., Chapman, J. M., Habing, H. J., Killeen, N. E. B., & Lindqvist, M. 1997a, A&AS, 122, 79

—. 1997b, A&AS, 124, 509

Sevenster, M. N., van Langevelde, H. J., Moody, R. A., et al. 2001, A&A, 366, 481

Sjouwerman, L. O., Habing, H. J., Lindqvist, M., van Langevelde, H. J., & A., W. 1999, "The Central Parsecs of the Galaxy" ASP Conf. Series 186 (p. 379)

Sjouwerman, L. O., van Langevelde, H. J., Winnberg, A., & Habing, H. J. 1998, A&AS, 128, 35

van Loon, J. T., Gilmore, G. F., Omont, A., et al. 2003, MNRAS, 338, 857

Vassiliadis, E. & Wood, P. R. 1993, ApJ, 413, 641

Whitelock, P., Feast, M., & Catchpole, R. 1991, MNRAS, 248, 276

Whitelock, P., Marang, F., & Feast, M. 2000, MNRAS, 319, 728

Whitelock, P., Menzies, J., Feast, M., et al. 1994, MNRAS, 267, 711

Whitelock, P. A., Feast, M. W., van Loon, J. T., & Zijlstra, A. A. 2003, MNRAS, 342, 86

Winfrey, S., Barnbaum, C., Morris, M., & Omont, A. 1994, Bulletin of the American Astronomical Society, 26, 1382

Wood, P. R., Habing, H. J., & McGregor, P. J. 1998, A&A, 336, 925

Zoccali, M., Renzini, A., Ortolani, S., et al. 2003, A&A, 399, 931